

The limit of spectral resolution in THz time-domain spectroscopy

Samuel Mickan^a, Jingzhou Xu^b, Jesper Munch^c, X.-C. Zhang^b and Derek Abbott^a

^aCentre for Biomedical Engineering, School of Electrical & Electronic Engineering, The University of Adelaide, Australia;

^bCenter for Terahertz Research, Rensselaer Polytechnic Institute, Troy NY, USA;

^cDepartment of Physics & Mathematical Physics, The University of Adelaide, Australia.

ABSTRACT

This paper describes a study conducted into the limit on spectral resolution due to the dynamic range of a T-ray spectrometer. The pulsed nature of terahertz time-domain spectroscopy (THz-TDS) sets a fundamental limit on its spectral resolution. The spectral resolution of THz-TDS can be improved by increasing the duration of the temporal measurement, but is limited by the dynamic range of the system in the time-domain. This paper presents calculations and experimental results relating the temporal dynamic range of a THz-TDS system to its spectral resolution. We discuss three typical pulsed terahertz sources in terms of their dynamic range and hence achievable spectral resolution.

Keywords: T-rays, terahertz (THz) time-domain spectroscopy, ultrafast photonics

1. INTRODUCTION

1.1. Motivation

T-ray Time-Domain Spectroscopy (TDS) is an innovative sensing and imaging technology for generating electromagnetic radiation at terahertz (THz) frequencies. The T-ray band is defined as 0.1 to 10 THz. T-ray spectroscopy provides information unavailable through conventional methods, such as microwave and X-ray techniques. To optimise T-ray spectroscopy, efforts have been made to extend the bandwidth^{1,2} and improve the signal-to-noise-ratio (SNR) of T-ray systems.^{3,4}

A desirable characteristic of any spectroscopy measurement is high spectral resolution, which is critical for observing resonances with narrow line widths, associated with distinct energy transitions at T-ray frequencies.⁵ Molecular absorption resonances have linewidths of approximately 1 to 3 GHz (1 to 3 cm⁻¹) for vapour rotational modes⁶ or vibrational modes in simple biomolecules.⁷

This paper reviews the fundamental dependencies of spectral resolution in TDS and shows how a typical T-ray system is fundamentally limited by its SNR, or more specifically the *dynamic range* (the ratio of T-ray signal to probe beam noise).

1.2. Previous studies

In T-ray TDS, the spectrum is calculated by a numerical Fast Fourier Transformation (FFT) from the measured temporal waveform, $y(t)$. The measured waveform is a series of N discrete values $y(n)$ sampled at time intervals of t_s seconds, that is,

$$y(n) = y(t = nt_s), \quad n = 0 \dots N.$$

The spectrum is also a discrete set of values,

$$Y(k) = \text{FFT}(y(n)), \quad k = 0 \dots N.$$

Further author information: Samuel Mickan (corresponding author), Email: samuel.mickan@adelaide.edu.au, Tel: +61.8.8303.4115; Jingzhou Xu, Email: xuj@rpi.edu; Jesper Munch, Email: jesper.munch@adelaide.edu.au; X.-C. Zhang, Email: zhangxc@rpi.edu; Derek Abbott, Email: dabbott@eleceng.adelaide.edu.au

From Fourier theory, a higher spectral resolution Δf is obtained by extending the temporal measurement window T , which corresponds to the scanning distance – that is

$$\Delta f \approx \frac{1}{T}, \quad (1)$$

where $T = (N - 1)t_s$.

The duration of the temporal measurement window is limited by one of three experimental considerations: (i) the repetition rate f_{laser} of the laser source (used to generate and detect T-ray pulses), (ii) the length of the scanning delay stage L that translates into a scanning duration T , and (iii) the amount of noise in the measurement.

The time duration between consecutive pulses, $1/f_{\text{laser}}$, can be improved upon by using a lower repetition rate laser amplifier rather than higher repetition rate laser oscillator.

The length L of the scanning delay can be extended by using alternative time scanning methods to replace distance scanning.

The limitation due to noise in the measurement is the most difficult to overcome, and therefore tends to be the fundamental limitation on frequency resolution in T-ray spectroscopy measurements.

The noise in T-ray TDS arises from two sources, fluctuations in the T-ray radiation $N_T(t)$ and fluctuations in the laser probe beam $N_B(t)$.⁸ The contributions of these noise sources, and their dependence on the temporal measurement duration, are described in Sec. 2. The physical sources of T-ray noise and probe beam noise are discussed in other publications.⁶

1.3. Objective summary

In this paper, the spectral resolution of time-domain spectroscopy is shown to be limited by the temporal dynamic range of a T-ray spectrometer, which is fundamentally limited by the *dynamic range*, or signal-to-noise ratio (SNR) caused by the laser probe beam.

The relationship between the dynamic range and the achievable frequency resolution is demonstrated with calculations and experimental data.

2. THEORY

In T-ray spectroscopy, the temporal waveform of the T-ray pulse $y(t)$ is sampled at temporal intervals of t_s over a range of T .

Any sampled T-ray waveform includes the electric field of T-ray radiation $E_T(t)$, noise due to fluctuations in the T-ray field $N_T(t)$ and background noise from the T-ray detection (probe) beam, $N_B(t)$:

$$y(t) = E_T(t) + N_T(t) + N_B(t). \quad (2)$$

In T-ray TDS, the time-domain waveform $y(t)$ is measured at a series of points from $t = 0$ to $t = T$. The waveform samples are uniformly spaced by a time t_s over the duration $T = (N - 1)t_s$, where N is the total number of samples. The waveform is therefore represented by the discrete series:

$$y(n) = E_T(n) + N_T(n) + N_B(n), \quad (3)$$

for $n = 0$ to $N - 1$.

The electric field of the T-ray radiation, E_T , occurs as a pulse, with a duration τ of approximately $\tau \approx 1$ to 10 ps. The pulse has a sharp rise time and decay in the first few ps, followed by a low amplitude decay. The exact form of the T-ray pulse depends on the T-ray emitter, the most common of which are Photoconductive Dipole Antennas (PDAs), semiconductor wafers exhibiting Surface Current Generation (SCG), and electro-optic crystals exhibiting Optical Rectification (OR). Equations that model the shape of these generated T-ray waveforms are

Table 1: The temporal waveform of the T-ray pulse depends mainly on the generation and detection mechanism and varies from one T-ray spectrometer to another. The waveforms may be simulated using several simple formulas. This Table lists the temporal waveforms ($E_T(t)$) for T-ray pulses generated by three common sources of pulsed T-ray radiation: (i) a Photoconductive Antenna (PCA), which has a bi-polar waveform; (ii) an unbiased semiconductor and Surface Current Generation (SCG), which has a unipolar waveform; and (iii) Optical Rectification (OR), which has a decaying oscillation. In these models, A is the maximum amplitude of the T-ray field (in A.U. or Volts), τ represents the pulse duration (in s), t is time (in s), and ω_0 is the oscillation frequency (in rad/s) and a is the decay constant (a function of τ) of generated beam in OR. (These equations are taken from Ref. 8.)

T-ray source	Model generated waveform
PCA	$2A\frac{t}{\tau^2} \exp(-t^2/\tau^2)$
SCG	$\frac{2A}{\tau^2} \exp(-t^2/\tau^2) - 4A\frac{t^2}{\tau^4} \exp(-t^2/\tau^2)$
OR	$A \sin(\omega_0 t) \exp(-at), \quad t > 0$ $0, \quad t \leq 0$

Table 2: This Table lists the temporal spectra ($E_T(\omega)$) for T-ray pulses generated by three common sources of pulsed T-ray radiation: (i) Photoconductive Antenna (PCA), (ii) Surface Current Generation (SCG), and (iii) Optical Rectification (OR). These equations are obtained by Fourier theory from the time-domain pulse models in Table 1. In these models, A is the maximum amplitude of the T-ray field (in A.U. or Volts), τ represents the pulse duration (in s), ω is frequency (in rad/s), and ω_0 is the oscillation frequency (in rad/s) and a is the decay constant (a function of τ) of generated beam in OR. (These equations are taken from Ref. 8.)

T-ray source	Model generated spectra
PCA	$A \frac{\omega\tau}{\sqrt{2}} \exp(-\omega^2\tau^2/4)$
SCG	$A \frac{\omega^2\tau}{\sqrt{2}} \exp(-\omega^2\tau^2/4)$
OR	$A \sqrt{\frac{\omega_0^2}{[a^2+(\omega_0-\omega)^2][a^2+(\omega_0+\omega)^2]}}$

listed Table 1, and an example simulated PCA waveform is shown in Fig. 1. The energy of E_T is concentrated in the initial part of the pulse, $t \approx \tau$, as shown in the example energy waveform in Fig. 2.

Currently, T-ray radiation for most systems is generated by photo-switching⁹ or Optical Rectification.¹⁰ The temporal waveform of the T-ray pulse generated by photo-switching may be described as either bipolar (with an outer electrical field) or unipolar (with an inner electrical field). The temporal waveform of the T-ray pulse generated by Optical Rectification (OR) is considered as a damped oscillation.

The noise in the T-ray beam, N_T , is caused by fluctuations in T-ray generation, due to pump beam noise. This noise has a zero mean, a $1/f$ spectral distribution and is proportional to the T-ray electric field at each moment in time, $N_T(t) \propto E_T(t)$. As it is proportional to the T-ray electric field, the energy in the T-ray noise is concentrated in the same duration, that is $t \approx \tau$. For short measurement durations, the noise in the T-ray beam dominates the noise in the probe laser beam. However, for large values of T , the noise in the probe beam makes a larger contribution. This paper is a study of SNR for large values of T , thus the effect of N_T can be neglected in comparison to the effect of N_B .

The noise in the laser probe beam, N_B , is directly due to laser fluctuations and is zero-mean, Gaussian white noise with a variance of σ_B . Unlike N_T , the noise in the probe beam is not dependent on the T-ray power. For large T , the contribution of probe beam noise dominates the T-ray noise.

The *dynamic range* is the ratio of the T-ray signal to the probe beam noise,

$$\text{dynamic range} = \frac{N_B}{E_T}. \quad (4)$$

The two contributions to the dynamic range, E_T and N_B , are shown in Fig. 1 as waveforms in the time-domain. The T-ray pulse has a high initial amplitude that quickly dies away. The probe beam noise has a low but constant amplitude and a Gaussian probability distribution.

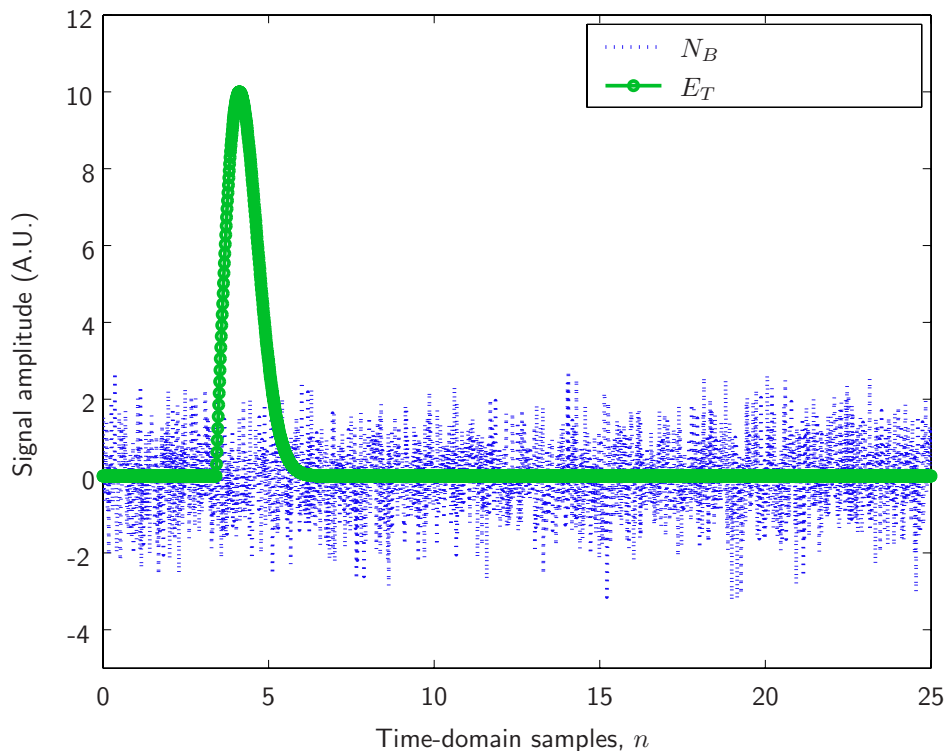


Figure 1: This Figure shows a portion of a simulated T-ray signal E_T and accompanying probe beam noise N_B . The T-ray waveform shows a sharp rise and fall, while the probe beam noise shows a lower but constant amplitude with a Gaussian probability distribution. These waveforms were simulated using the time-domain equation for a PCA pulse in Table 1 and the `randn` random Gaussian noise generation function in MATLAB. The parameters for this simulation are shown in Table 3.

The contribution of E_T is greater than N_B or N_T at small values of T (when T is approximately equal to the signal duration τ). However, at large values of T , the contribution of N_B begins to dominate. The contribution of N_T falls in proportion to E_T , so for low values of E_T at large t , N_B dominates.

Table 3: The parameters used in the simulation are listed in Col. 1, and the values used in this simulation are in Col. 2. The simulated pulse from a PCA was modelled using the equation in Table 1. The values listed in this table are similar to those used in T-ray experiments. The dynamic range is the ratio of T-ray pulse amplitude to probe beam noise amplitude. The stage scan length is the distance travelled by the delay state in a T-ray spectrometer L that would create a scan time of T ; the $1/2$ factor is caused by the optical delay being double the physical translation of the stage.

Parameter	Symbol	Value
Dynamic range	A/σ_{B-t}	10 V/V
Pulse duration	τ	5 ps
Sample separation	t_s	66.67 fs
No. of samples	N	16,384 (2^{14}) points
Scan time	$T = t_s(N - 1)$	1.09 ns
Stage scan length	$L = T c_0/2$	16.3 cm

The contributions of E_T and N_B can be compared in terms of energy. Figure 2, the energy waveform, shows that for large values of t , the noise in the probe beam makes a larger contribution to the energy in the measurement than the signal E_T . This result shows that increasing the value of T will lead to an eventual reduction in overall signal-to-noise ratio. Thus the fundamental limit on spectral resolution in T-ray TDS, $\Delta f \approx 1/T$, is caused by the probe beam noise.

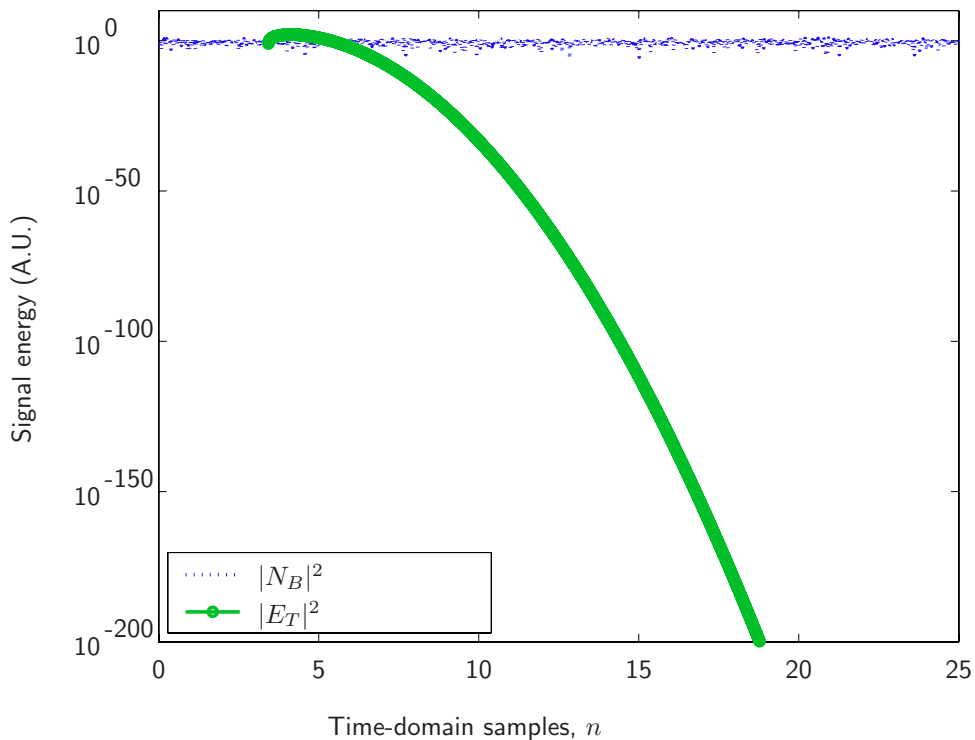


Figure 2: The plots of probe beam noise energy $|N_B|^2$ and T-ray signal energy $|E_T|^2$ show the energy in the signal and beam noise as a function of time $n = t/t_s$. The T-ray signal has most of its energy in the initial part of the pulse, with very little energy remaining for larger times. The average energy in the probe beam noise is constant over time. These plots are obtained by taking the amplitude of the waveforms in Fig. 1.

The limit of acceptable SNR in an experiment depends on the measurement being made, but there will be some limit beyond which the signal of interest is obscured.

The SNR in an experiment can be quantified in the time domain by comparing the total sum of the signal energy $\sum_0^{N-1} |E_T|^2$ to the sum of the noise energy $\sum_0^{N-1} (|N_T|^2 + |N_B|^2)$. As a larger value of T is chosen, the total contribution due to N_B will rise while the signal power remains approximately constant. At some point the accumulated noise energy (from the probe beam) will be greater than the accumulated T-ray energy, and the average frequency signal will be obscured by noise.

The cumulative contributions of T-ray power and probe beam noise can be compared by summing the energy over each scan: Fig. 3 shows the total signal and noise energies as a function of increasing T .

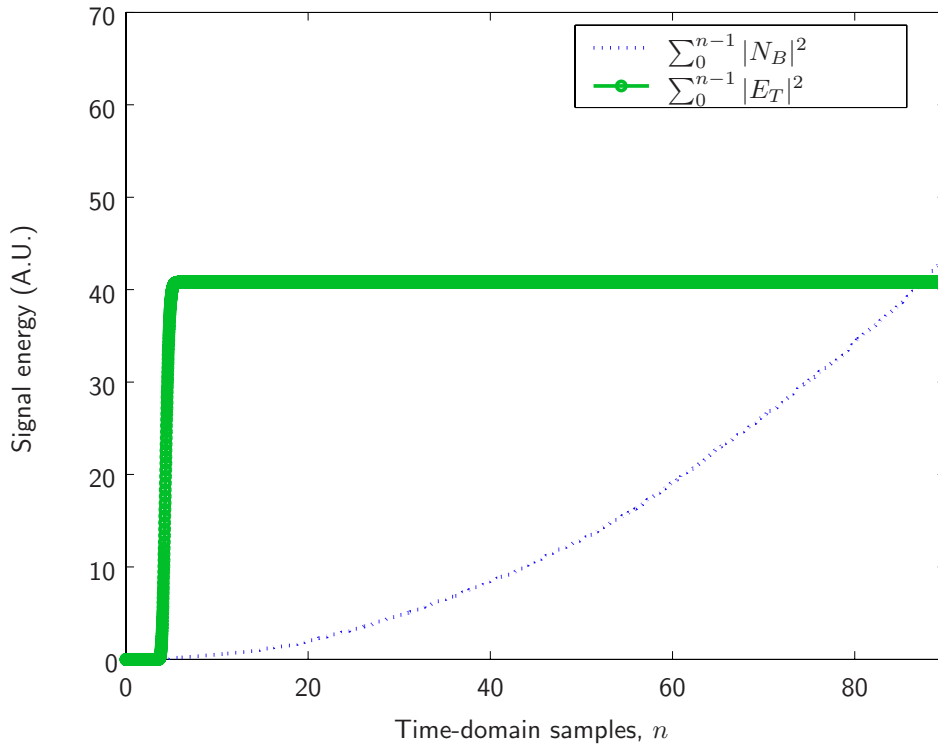


Figure 3: The plots in this graph show the accumulation of energy over a measurement time $n = t/t_s$: accumulated probe beam noise energy $\sum_0^{n-1} |N_B|^2$, and accumulated T-ray signal energy $\sum_0^{n-1} |E_T|^2$. These simulated graphs are obtained by numerically integrating the graphs in Fig. 2, but the time scale has been extended to show the point where the accumulated probe beam noise energy equals the accumulated T-ray signal energy: at this point the average signal-to-noise ratio (due to probe beam noise) = 1. The vertical axis values have been scaled down by 10^6 for clarity.

The point in Fig. 3 where the two curves cross corresponds to the duration at which the total T-ray signal energy equals the total noise energy in the probe beam. Thus, at the cross-over point, the average SNR of the T-ray spectrum is 1.0.

The average SNR of a spectroscopy measurement depends on the temporal measurement duration T . However, T-ray TDS is typically used to study specific frequency ranges, depending on the frequencies of interest – for example, specific absorption modes in gas molecules, or the dielectric constant of a material in a specific frequency range. To show the SNR of a measurement in a specific frequency range, and how it depends on T , the spectra of a T-ray pulse (in this case simulated from a PCA) and the probe beam noise are shown in Fig. 4. This Figure

shows that the SNR of the spectrum is different for different frequencies, thus the average SNR (as calculated in the time domain) is less important than the SNR at a specific frequency of interest.

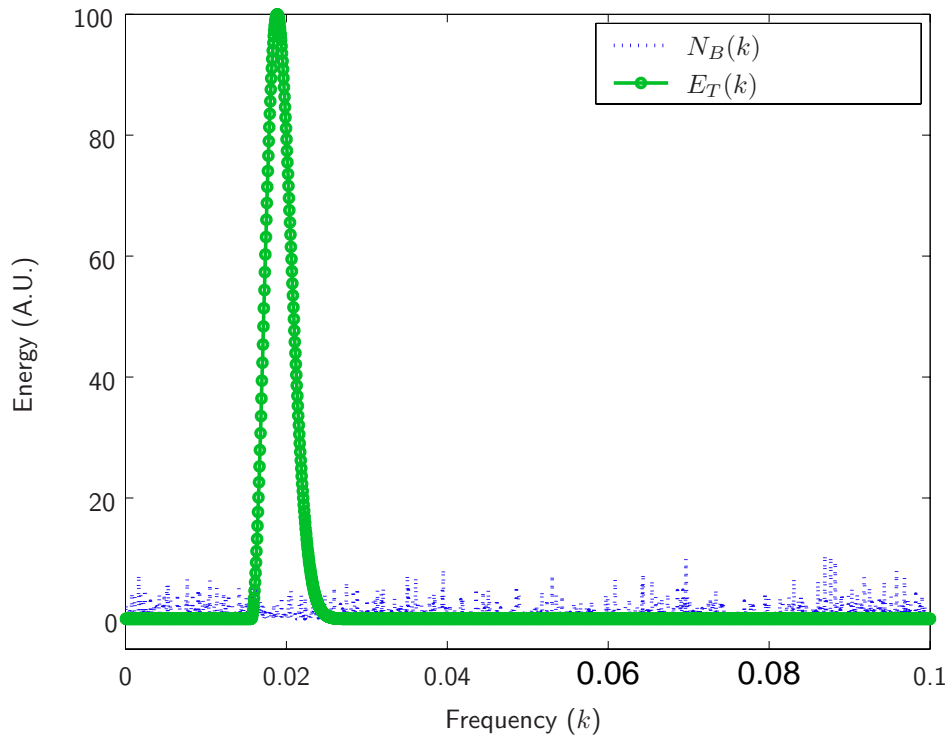


Figure 4: This graph shows a portion of the sampled (amplitude) spectra of the T-ray signal $E_T(k)$ and the probe beam noise $N_B(k)$. Most of the T-ray energy lies in a narrow part of the spectrum while the Gaussian white probe beam noise is distributed equally across all frequencies, thus the SNR of interest depends on the frequency range of interest. The spectra in this graph were obtained using a numerical Fast Fourier Transform (FFT) in MATLAB of the temporal waveforms in Fig. 1.

In T-ray TDS, the spectrum of T-ray pulse energy, $E_T(\omega)$, is represented by a discrete frequency domain data series, $E_T(k)$, where $k = 0$ to $N - 1$. The frequency spacing of the points, Δf , equals $1/T$ (from Fourier theory). The T-ray signal power at a given frequency, for example f_1 , can be seen through measurement (using the FFT, as in Fig. 4) or calculation (using the expressions in Table 1) of the spectrum of the T-ray pulse, $E_T(\omega = 2\pi f_1)$.

From Fourier theory, it can be shown that the mean of the probe beam noise in the frequency domain, and its variance $\sigma_{B-\omega}^2$, depend on the variance in the time domain, σ_{B-t}^2 , and the number of points in the FFT, N^{11} :

$$\sigma_{B-\omega}^2 = N \sigma_{B-t}^2. \quad (5)$$

From the discussion of an increased contribution from probe beam noise for long scanning times, it is not surprising that the mean level of the noise, and its variance, are proportional to N , as shown in Eq. (5).

The maximum frequency resolution of a measurement at a frequency of interest, for example f_1 , is determined by the length of T , which is in turn determined by the acceptable SNR at f_1 in the frequency spectrum.

For a sample with a material absorption of strength $M(\omega)$, an SNR of at least $1/M(\omega)$ is required. For a time-domain probe beam of variance of σ_{B-t}^2 (which can be measured), the maximum frequency resolution at f_1 will be given by

$$\Delta f_{\min}(f_1) = 1/T_{\max},$$

where T_{\max} is the value of T such that the T-ray signal energy at f_1 equals $M(\omega = 2\pi f_1)$ -times the noise energy at f_1 , that is,

$$|E_T(f_1)|^2 = \frac{1}{M(f_1)} N \sigma_{B-t}^2. \quad (6)$$

Thus since $N = T/t_s$,

$$T_{\max} = \frac{t_s |E_T(f_1)|^2 M(f_1)}{\sigma_{B-t}^2}. \quad (7)$$

An example limit on Δf , using Eq. (7) with realistic experimental quantities, is given in Sec. 4.

The dependence of the SNR at a frequency of interest (f_1) can be expressed as a function of T :

$$\begin{aligned} \text{SNR}(f_1) &= \frac{E_T(f_1)}{\sigma_{B-\omega}} \\ &= \frac{\sqrt{t_s} E_T(f_1)}{\sqrt{T} \sigma_{B-t}}. \end{aligned} \quad (8)$$

For a given time-domain probe beam variance σ_{B-t}^2 and sampling interval t_s , the signal-to-noise ratio at a given frequency is inversely proportional to the square root of the scanning range T . This result is confirmed experimentally in the following Section.

3. EXPERIMENTS

To demonstrate experimentally the relationship between the dynamic range in the frequency domain and temporal scanning range, a T-ray waveform was measured using a femtosecond laser and a 2-mm-thick ZnTe crystal.¹² The emitted T-ray wave was collimated and focused by two parabolic mirrors and detected using Electro-Optic Sampling (EOS) by a 5-mm-thick ZnTe crystal.¹⁰ The entire T-ray beam path was purged by dry air and the humidity was limited to less than 6%; water vapour absorption was not considered to be significant in these experiments. The delay stage resolution in the experiment was 10 μm (66.67 fs) and the temporal measurement dynamic range was 1000.

A series of T-ray spectra were extracted by numerical Fourier transform (FFT) of the temporal waveforms in the range of 0 to $2^n T_0$, where $T_0 = 8.53$ ps and $n = 0, 1, \dots, 11$. That is, 12 measurements were made, each with a duration ranging from 0 to $2^n T_0$. The different duration measurements were designed to measure different amounts of background noise.

4. RESULTS

The signal-to-noise ratio at the frequency with the maximum amplitude (f_1) is presented as a function of temporal scanning range in Fig. 5. The solid dots are experimental data and the curve is fitted by Eq. (8). The SNR in the frequency domain is inversely proportional to the square root of the temporal scan duration, as predicted by the theory in Sec. 2.

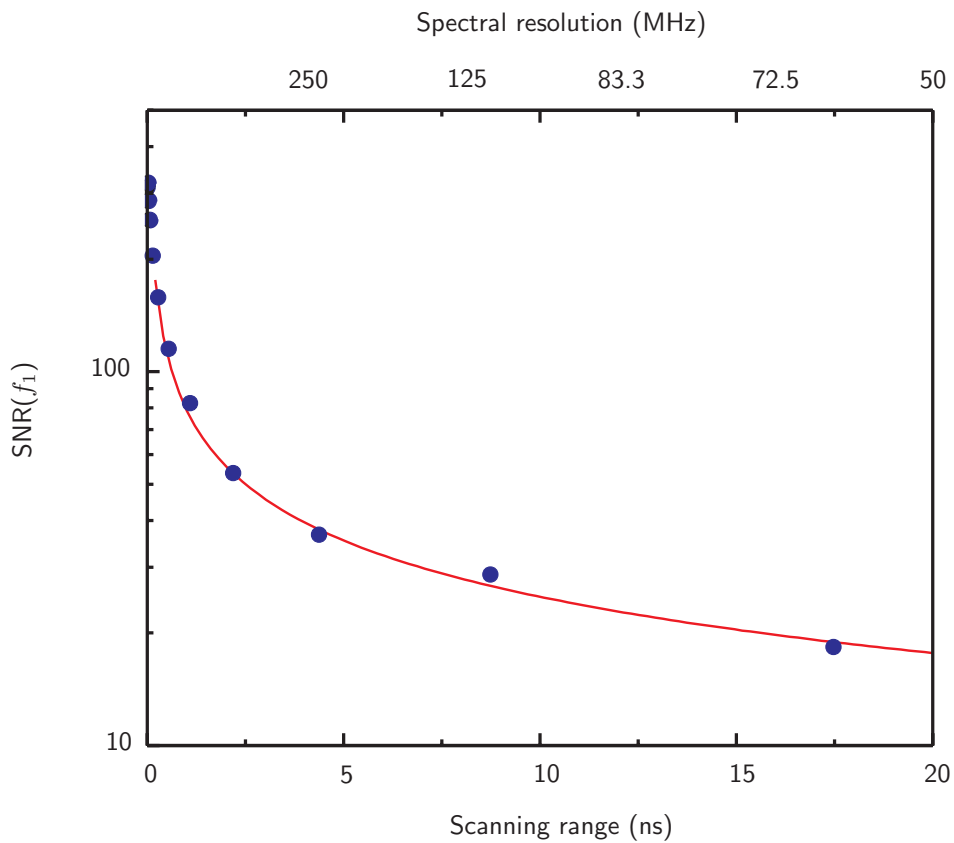


Figure 5: This graph shows the variation of the SNR of T-ray TDS at one frequency as a function of the temporal scanning range T . The frequency chosen for these measurements was the frequency that had the highest amplitude. The solid dots are experimental data and the curve is fitted the calculated results from Eq. (8), thus confirming its accuracy. The experimental conditions are described in Sec. 3. The spectral resolution Δf is also shown in this graph, and is inversely proportional to the scanning range T .

For a generated T-ray spectrum from a PCA, such as in Fig. 4, the spectral shape can be modelled using the equation for a PCA in Table 2,

$$E_T(\omega) = A \frac{\omega\tau}{\sqrt{2}} \exp -\omega^2\tau^2/4. \quad (9)$$

From Eq. (9), Eq. (7), and $\Delta f = 1/T_{\max}$, the best frequency resolution for a sample with absorption $M(\omega)$ can be expressed as

$$\begin{aligned} \Delta f_{\min} &= \frac{1}{T_{\max}} \\ &= \sigma_{B-t}^2 / \left(\sqrt{2t_s M(f_1)} A \pi f_1 \tau \exp[-\pi^2 f_1^2 \tau^2] \right)^2. \end{aligned} \quad (10)$$

For example, for a sample with $M(f_1) = 1\%$ at a frequency of interest $f_1 = 0.18$ THz, probed with a T-ray spectrometer (sampled at $t_s = 66.67$ fs) using a PCA emitter (pulse duration $\tau = 5$ ps, spectrum from Table 2) and a measured dynamic range $A/\sigma_{B-t} = 10^6$, the highest spectral resolution of the T-ray spectrometer is approximately 0.8 GHz.

5. CONCLUSION

In summary, this paper has demonstrated that the spectral resolution of T-ray spectroscopy depends not only on the duration of the sampled time-domain waveform $y(t)$, but more fundamentally on the *dynamic range* of the T-ray spectrometer. A high dynamic range system is required for high-resolution spectroscopy.

For a typical spectroscopy system limited by probe beam noise, an achievable resolution of approximately 0.8 GHz is achievable at around 0.5 THz. This compares favourably to molecular linewidths, which are of the order of 1 GHz. For higher frequency measurements, broadband T-ray generation using Surface Current Generation (SCG) or Optical Rectification (OR) is required.^{13,14}

5.1. Future work

For high-resolution T-ray spectroscopy, the ratio of T-ray power to laser probe beam power must be maximised. Research is ongoing into high-power T-ray sources based on PCAs¹⁵ and electron beams.¹⁶ Noise in the probe beam can be reduced by using stable solid-state-pumped ultrafast lasers,¹⁷ by hard-limiting the output power of the laser¹⁸ and by using longer integration times (signal averaging).

ACKNOWLEDGMENTS

The authors would like to acknowledge the financial support of the US National Science Foundation, the US Army Research Office, and the Australian Research Council.

REFERENCES

1. R. Huber, A. Brodschelm, F. Tauser, and A. Leitenstorfer, "Generation and field-resolved detection of femtosecond electromagnetic pulses tunable up to 41 THz," *Applied Physics Letters* **76**, pp. 3191–3193, 2000.
2. S. Kono, M. Tani, and K. Sakai, "Coherent detection of mid-infrared radiation up to 60 THz with an LT-GaAs photoconductive antenna," *IEE Proceedings Optoelectronics* **149**, pp. 105–109, 2002.
3. L. Duvillaret, F. Garet, and J. L. Coutaz, "Influence of noise on the characterization of materials by terahertz time-domain spectroscopy," *Journal of the Optical Society of America B: Optical Physics* **17**(3), pp. 452–461, 2000.
4. S. P. Micken, K. S. Lee, T.-M. Lu, J. Munch, D. Abbott, and X.-C. Zhang, "Double modulated differential THz-TDS for thin film dielectric characterization," *Microelectronics Journal (Elsevier)* **33**(12), pp. 1033–1042, 2002.
5. M. C. Beard, G. M. Turner, and C. A. Schmuttenmaer, "THz spectroscopy," *Journal of Physical Chemistry B* **106**, pp. 7146–7159, 2002.

6. M. van Exter and D. Grischkowsky, "Characterization of an optoelectronic terahertz beam system," *IEEE Transactions on Microwave Theory and Techniques* **38**(11), pp. 1684–1691, 1990.
7. M. Walther, B. Fischer, M. Schall, H. Helm, and P. U. Jepsen, "Far-infrared vibrational spectra of all-trans, 9-cis and 13-cis retinal measured by THz time-domain spectroscopy," *Chemical Physics Letters* **332**(3–4), pp. 389–395, 2000.
8. J. Xu, T. Yuan, S. P. Micken, and X.-C. Zhang, "Limits of spectral resolution in terahertz time-domain spectroscopy," *Chinese Physics Letters* **20**(8), pp. 1266–1268, 2003.
9. D. H. Auston, K. P. Cheung, and P. R. Smith, "Picosecond photoconducting Hertzian dipoles," *Applied Physics Letters* **45**(3), pp. 284–286, 1984.
10. Q. Wu and X.-C. Zhang, "Free-space electro-optic sampling of terahertz beams," *Applied Physics Letters* **67**(24), pp. 3523–3525, 1995.
11. J. G. Proakis and D. G. Manolakis, *Digital Signal Processing: Principles, Algorithms, and Applications*, Prentice-Hall, Upper Saddle River, NJ, U.S.A., 3rd ed., 1996.
12. X.-C. Zhang, Y. Jin, K. Yang, and L. J. Schowalter, "Resonant nonlinear susceptibility near the GaAs band gap," *Physical Review Letters* **69**(15), pp. 2303–2306, 1992.
13. P. Y. Han and X.-C. Zhang, "Coherent, broadband midinfrared terahertz beam sensors," *Applied Physics Letters* **73**(21), pp. 3049–3051, 1998.
14. A. Leitenstorfer, S. Hunsche, J. Shah, M. C. Nuss, and W. H. Knox, "Detectors and sources for ultra-broadband electro-optic sampling: Experiment and theory," *Applied Physics Letters* **74**(11), pp. 1516–1518, 1999.
15. G. Zhao, R. N. Schouten, N. van der Valk, W. T. Wenckebach, and P. C. M. Planken, "A terahertz system using semi-large emitters: Noise and performance characteristics," *Physics in Medicine and Biology* **47**(21), pp. 3699–3704, 2002.
16. G. P. Williams, "Far-IR/THz radiation from the Jefferson Laboratory, energy recovered linac, free electron laser," *Review of Scientific Instruments* **73**(3), pp. 1461–1463, 2002.
17. J. A. Moon, "Optimization of signal-to-noise ratios in pump-probe spectroscopy," *Review of Scientific Instruments* **64**(7), pp. 1775–1778, 1993.
18. C. Zhang, K.-S. Lee, X.-C. Zhang, X. Wei, and Y. R. Shen, "Optical constant of ice Ih crystal at terahertz frequencies," *Applied Physics Letters* **79**(4), pp. 491–493, 2001.